Nanoscale Advances

ROYAL SOCIETY OF CHEMISTRY

PAPER

View Article Online
View Journal | View Issue

Cite this: *Nanoscale Adv.*, 2026, **8**, 1228

Exfoliation and transfer of millimetre-sized MoS_2 flakes on arbitrary substrates

Riccardo Galafassi, †*[ab] Ermes Peci, †[c] Valentina Venturino, [c] Michele Magnozzi, [c] Francesca Telesio, [d] Maurizio Canepa [c] and Francesco Bisio [a]

Two-dimensional (2D) materials have the potential to strongly and sustainably influence technological development in the fields of optoelectronics, energy production and management, catalysis and more. One limiting factor that presently prevents the full exploitation of these materials is, however, the difficulty of obtaining large-scale, high-quality 2D samples on arbitrary substrates. In this work, we introduce a significant generalization of previously reported gold-assisted exfoliation techniques for TMDCs, marking a step forward towards the fabrication of macroscopic 2D material samples on arbitrary substrates. We achieved the successful production of millimetre-sized monolayer MoS_2 onto silica, PDMS, and both thermal and native oxidized silicon wafers. Moreover, our method simplifies previously reported gold-assisted exfoliation methods by removing substrate functionalization procedures and complex steps to achieve a reliable and reproducible procedure. The crystal quality of the monolayers was probed using XPS, Raman and photoluminescence spectroscopies, revealing a negligible presence of contaminants and defects in the samples. Furthermore, using imaging ellipsometry, we could investigate, on the millimetre scale, the sample morphology and the selectivity of the exfoliation process to produce single layer MoS_2 flakes. Finally, we further extended the capability of our exfoliation method by enabling the seamless transfer of large-area samples from PDMS to advanced substrates, unlocking new possibilities for large-scale 2D device fabrication.

Received 26th September 2025
Accepted 24th November 2025

DOI: 10.1039/d5na00919g

rsc.li/nanoscale-advances

Introduction

Ever since the first isolation of graphene,[1] 2-dimensional (2D) materials have become almost ubiquitous in condensed matter physics due to their amazing physical properties and ease of fabrication.[2] Among the large family of 2D materials, group-VI transition metal dichalcogenides (TMDCs) have drawn particular interest due to their semiconducting nature, excellent optoelectronic properties and widespread availability.[3] Their 2D character indeed promotes the appearance of unique properties, among which are the indirect-to-direct band gap transition when going from bulk to monolayer,[4] very high exciton binding energies[5] and spin-valley coupling in the electronic structure.[6] A wide range of possible applications arise from these outstanding properties, laying the ground for a possible technological revolution in fields such as electronics, optics, and computing.[7,8]

One of the major obstacles for the full exploitation of 2D systems has always been the lack of a scalable and reliable method for the deterministic production of spatially extended and high-quality monolayers. The most widely employed fabrication methods, such as the mechanical Scotch tape method,[1] liquid phase exfoliation,[9] and chemical vapor deposition,[10] all exhibit some intrinsic drawbacks in terms of either yield, scalability, or sample quality. Recent studies have shown great progress in this direction, reporting for example the wafer-scale growth of 2D materials, albeit with multiple translational grain boundaries;[11–13] a recently reported method based on 2D Czochralski growth also promises to address these issues by producing almost defect-free extended monolayers,[14] but the true scalability and universality of these methods have yet to be fully demonstrated.

In general terms, however, the conceptual and practical simplicity of the mechanical exfoliation method remains unparalleled; for this reason, great curiosity surrounded the report of the breakthrough achievement of extended TMDC monolayer fabrication obtained by introducing metallic layers to complement the conventional Scotch-tape method.[15–22] The rationale behind this innovative approach is to perform the mechanical exfoliation of the TMDC from the parent crystal not directly by tape, but by means of a metallic layer, whose

[a]*CNR-SPIN, Corso Perrone 24, 16152 Genova, Italy. E-mail: riccardo.galafassi@cnr.it*
[b]*RAISE Ecosystem, Genova, Italy*
[c]*Optmatlab, Dipartimento di Fisica, Università degli Studi di Genova, Via Dodecaneso 33, 16146 Genova, Italy*
[d]*Dipartimento di Fisica, Università degli Studi di Genova, Via Dodecaneso 33, 16146 Genova, Italy*
† These authors contributed equally to this work.

adhesion to the TMDC surface is stronger than the TMDC's interlayer adhesion.[15] Experiments showed that large monolayer (1L) TMDC areas could be peeled from the parent crystal in this way, significantly improving with respect to the original metal-free version.

Following early implementations,[16,17,23] metal-assisted exfoliation has been gradually improved and refined,[19,20,24] to the point of producing high-quality millimetre-sized monolayer TMDCs on selected substrates. The interaction between gold surfaces and TMDCs has been described in various ways.[24] Some studies characterize it as 'covalent-like quasi-bonding'[25,26] or 'mixed vdW-covalent',[27] while others refer to it as physisorption/chemisorption[28] or simply as a 'strong' interaction.[15,29–32] The roles of strain[33,34] and electrostatics[35] have been investigated. Beyond gold, several other metals have been shown to effectively exfoliate a variety of 2D materials.[36–38] Nevertheless, gold remains the primary focus of most studies, as it is resistant to oxidation and can be readily grown.[27]

Liu *et al.*, in particular, perfected gold-mediated exfoliation to the point of exfoliating large-area 1L samples onto non-metallic substrates,[39] seemingly addressing the issues and limitations that were present in early studies. A crucial aspect of their procedure was the exploitation of a thermal release tape (TRT) as a vector to mechanically sustain the sacrificial Au layer during the exfoliation of the TMDC and the transfer to the target substrate. Upon pressing TRT/Au/TMDC on a substrate of choice, the TRT was released by heating the system, and the sacrificial layer was etched, leaving the TMDC 1L behind. A later study by Petrini *et al.*,[40] however, despite strictly adhering to Liu's recipe, reported systematic cracking and wrinkling of the metal layer due to heat-induced stress of the TRT polymer, resorting to functionalization of the target substrate with (3-aminopropyl)triethoxysilane (APTES) in order to increase the adhesive force between the substrate and the TMDCs and circumvent the issue.[40] The procedure, albeit introducing an extra fabrication step, ensured improved mechanical stability of the TMDC/metal stack and successfully yielded large-area monolayers of TMDC, incidentally promoting stronger adhesion to the target substrate, a factor that may be beneficial in subsequent processes that require sample sonication[41] or detrimental when further transfer is required.

In order to be able to fabricate large-area 1L flakes of TMDCs on a large variety of substrates and leave open the possibility to further transfer them onto other systems, we developed an improved version of previously reported sacrificial gold layer-assisted exfoliation methods[39,40] that significantly extends the range of applicability of large-scale exfoliation of TMDCs. In detail, the surface functionalization of the target substrate was replaced with a simple reversible mechanical constraint, a rigid PDMS layer, introduced during the critical TRT-release stage, thereby altogether avoiding the need for intermediate additional chemical processes and additional fabrication steps that might compromise the sample quality. With this approach, we demonstrated the possibility of achieving large-area TMDC 1Ls on substrates as diverse as Si wafers with native (2 nm) and thermal (300 nm) oxide, bulk fused silica and polydimethylsiloxane (PDMS). Moreover, by exploiting the successful exfoliation on PDMS, which distinguishes our method from nearly all previously reported metal-assisted exfoliation methods, we demonstrated that large-area 1L TMDC flakes could be further deterministically transferred onto a wide variety of other substrates with microscopic control over crystal positioning, exploiting well-established PDMS-based dry-transfer methods.[42,43]

Exfoliation of large-area monolayer MoS_2

In this work, we focused on a natural crystal of MoS_2 as the parent bulk material for exfoliation, since its generalization to the many other 2D materials that are compatible with gold-assisted exfoliation is straightforward.[25,39] Since substrate compatibility was reported to be a delicate issue within existing gold-assisted exfoliation reports,[40] we chose to address different target substrates, namely: (i) p-type silicon (resistivity ∼20 Ω cm) with native SiO_2 oxide (SiO_2(nat)/Si); (ii) n-type silicon (resistivity ∼20 Ω cm) with a thermally grown SiO_2 layer (SiO_2(285 nm)/Si); (iii) fused silica; (iv) polydimethylsiloxane (Sylgard 184 with a 10 : 1 cross-linker/curing agent ratio), chosen as representative of different domains of future applications in the fields of electronics, optics and flexible devices. The choice of the doping type for the silicon wafers was mainly driven by the availability of the silicon wafers.

Fig. 1 shows the different steps of the exfoliation process. (1) A 150 nm-thick gold film was deposited *via* sputtering onto a Si wafer previously cleaned in oxygen plasma for 5 minutes at 50 W in order to remove contaminants on the surface; no adhesion layer was deposited in order to ensure easy peeling in the subsequent step. (2) A Nitto Denko Revalpha RA-95LS(N) thermal release tape (TRT) was then placed directly on the gold coated wafer and used to pick up a centimetre-sized piece of the gold film from the silicon wafer. (3) The TRT-supported gold film was pressed onto a freshly cleaved bulk MoS_2 crystal. This step was performed in the shortest time possible, in order to prevent the contamination of the gold surface and the MoS_2 crystal from ambient air.[44] The TRT/Au stack was then peeled off the bulk MoS_2, stripping a monolayer MoS_2 in the process, and pressed onto the target substrate of choice.

At this stage, in order to release the sample, the TRT needs to be heated above 105 °C; normally, this results in the TRT bending away from the underlying substrate, lifting the thin MoS_2/Au layer and preventing its transfer.[40]

In this work, we prevented the detrimental TRT buckling by (4) fully covering the MoS_2/Au/TRT system by means of an adhesive rigid layer, thereby providing a mechanical constraint for the TRT and allowing it to lose adhesion while simultaneously maintaining the Au/MoS_2 assembly firmly in contact with the substrate. For our experiments, the constraint layer consisted of 1.5 mm-thick PDMS, which ensured surface cleanliness and prevented sample contamination. The PDMS

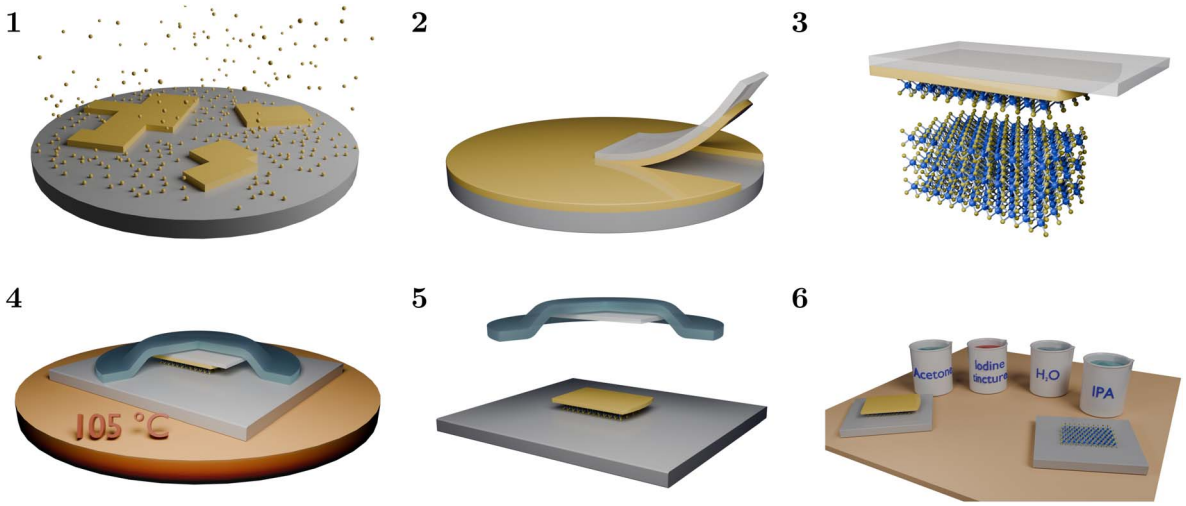

Fig. 1 Step-by-step schematic representation of the exfoliation process. (1) A 150 nm thick gold film is deposited *via* sputtering onto a silicon wafer. (2) Part of the gold layer is peeled off from the wafer by means of the TRT. (3) The gold/TRT stack is exploited to exfoliate a MoS_2 monolayer from the bulk crystal. (4) The MoS_2/Au/TRT system is laid on the desired substrate, pressed with a PDMS layer (light blue) and heated to promote the detachment of the TRT. (5) The MoS_2/Au stack is detached from the TRT. (6) The gold layer is etched by sequentially dipping the substrate/MoS_2/Au system in acetone, iodine tincture, H_2O and IPA.

was prepared using Sylgard 184 with a 10 : 1 cross-linker/curing agent ratio and cured for 24 hours at 60 °C. The PDMS was placed directly on the MoS_2/Au/TRT stack upon cutting a large enough region to fully cover the sample. (5) The PDMS/TRT stack was then removed, leaving the Au/MoS_2/substrate system behind, and (6) the gold layer was dissolved by standard Au-etching procedures: the sample was first washed in acetone for a few minutes to remove any organic contamination from the tape, then the gold layer was etched using iodine tincture (1 : 4 : 40 I_2 : KI : H_2O) and washed in DI water, in IPA, and finally dried using dry nitrogen.

Steps (2) to (4) were performed under a controlled nitrogen atmosphere in order to minimize the humidity level during the exfoliation procedure, effectively reducing airborne contamination of the Au/MoS_2 interface and consequently improving the exfoliation throughput.[44–46]

In SI, Fig. S1 shows photos of the various steps of the exfoliation procedure.

Imaging ellipsometry of large-scale monolayers

In Fig. 2, we show optical microscopy images of one representative sample for each substrate type. The samples on SiO_2(285 nm)/Si, fused silica and PDMS exhibit an optical contrast sufficiently high to be located under a normal optical microscope, while the flakes exfoliated on Si wafers with native oxide are not readily observable, as indeed expected.

In order to overcome this complication and, above all, to quantitatively assess the sample morphology, we performed imaging spectroscopic ellipsometry (iSE) measurements, which allow probing of the optical properties of 2D materials[47–49] and ready detection of sample thickness variations with sub-nanometre precision, unambiguously identifying the number of exfoliated layers[50] of TMDC systems. Moreover, in contrast with atomic force microscopy (AFM), which has proved to be inefficient in measuring the thickness of monolayer

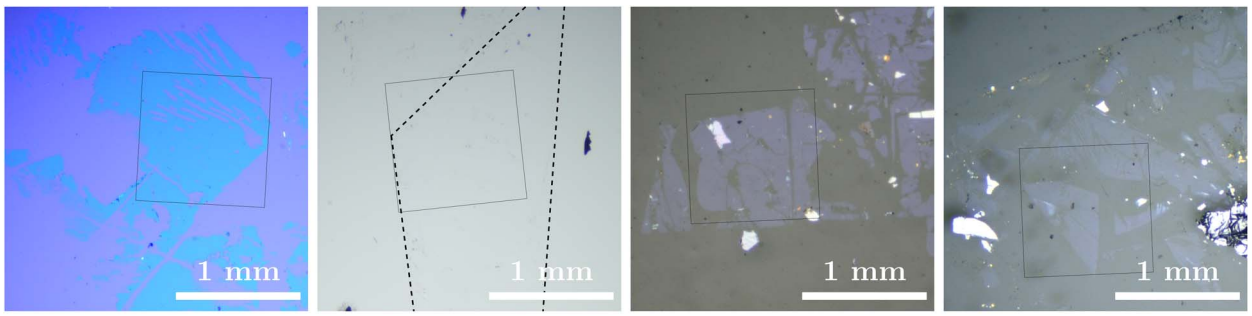

Fig. 2 Optical microscopy of the samples exfoliated on different substrates, as indicated in the panel caption. (a) 285 nm SiO_2/Si; (b) 2 nm SiO_2/Si; (c) PDMS; (d) fused silica The black rectangles indicate the area where imaging ellipsometry measurements were performed. In panel (b), where optical contrast is negligible, a black dashed line marks the approximate outline of the sample.

samples,[51,52] iSE thickness measurements are unaffected by the eventual presence of contaminants and by the interaction with the substrate that may lead to anomalous thickness values using AFM. Instead, the latter was used to image the surface topography and acquire information on the surface morphology of the samples. Fig. S4 displays the AFM map of a sample on SiO_2(nat)/Si, showing the absence of contaminants on the MoS_2 surface, beside small unavoidable dust particles. Hyperspectral iSE measurements were performed by mapping the ellipsometric angles $\Psi(\lambda)$ and $\Delta(\lambda)$ at 129 different wavelengths spanning the near-UV, visible and near-infrared ranges, as detailed in the Methods section. A few representative maps are reported in Fig. S2 and S3.

The experimental data were subsequently analysed by means of a layer-stack model that included, bottom to top, a semi-infinite substrate, a SiO_2 layer (where applicable) and a MoS_2 layer with a parameterized complex dielectric function adapted from our previous work[53] (Fig. 3a). For the latter, the tabulated optical constants can be found in the SI in Table S1. The full description of the model used for each system can be found in Fig. S5. Continuous lines in Fig. 3b show the values of Ψ and Δ as a function of the energy of the incoming light, averaged over the homogeneous regions highlighted by the dashed polygons

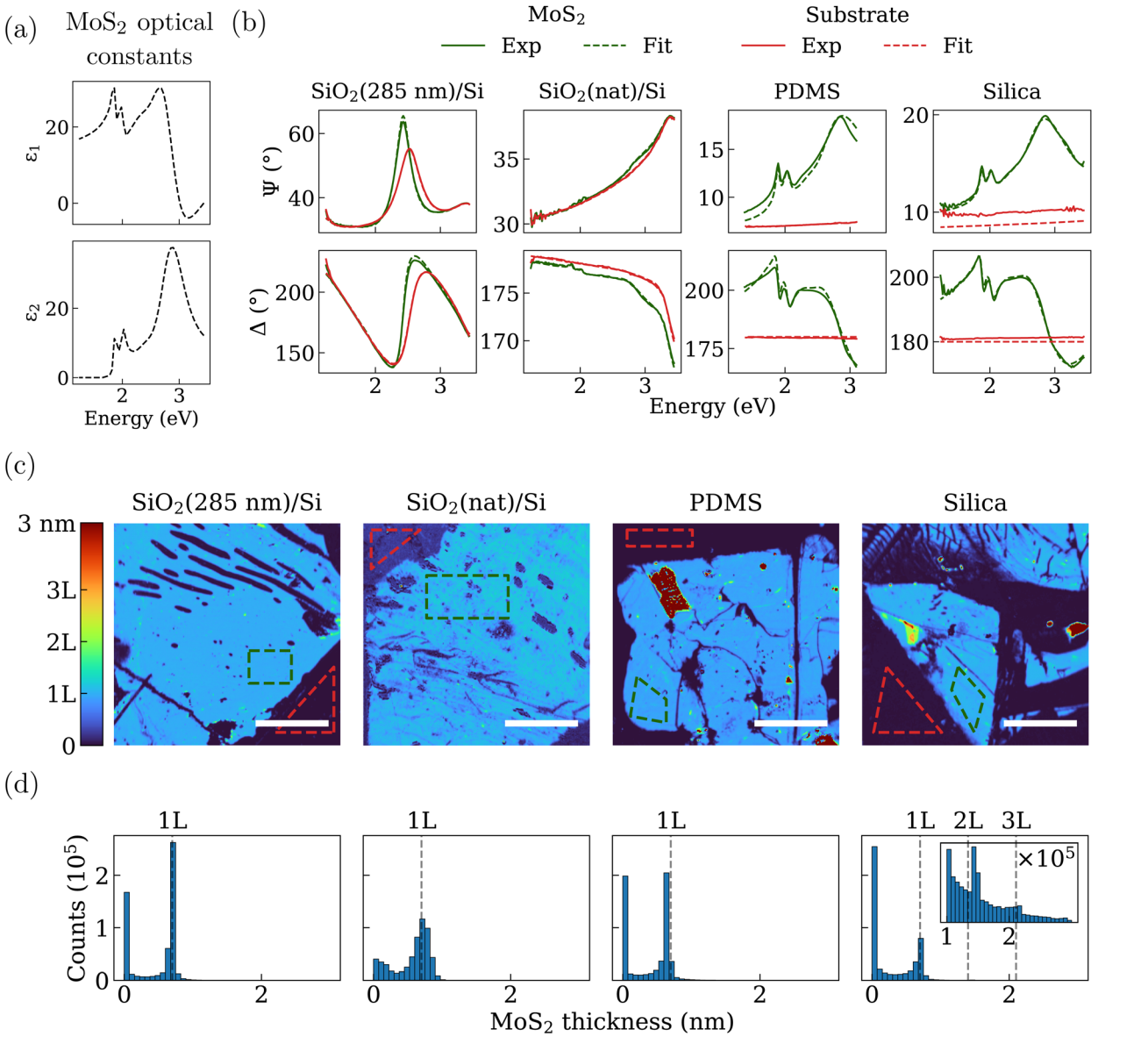

Fig. 3 (a) Optical constants of the MoS_2 used in the modelling.[53] (b) Experimental data (solid lines) and best fits (dashed lines) of the ellipsometric angles $\Psi(\lambda)$ and $\Delta(\lambda)$ averaged over the dashed-line regions of (c). The green lines correspond to MoS_2-covered regions, whereas the dark-red ones indicate the respective substrates. (c) MoS_2 thickness maps extracted from the analysis of the imaging ellipsometric measurements. Light blue areas correspond to exfoliated MoS_2 areas. Dark red regions in the samples on PDMS and silica indicate the presence of thick multilayer regions. The scale bar is 300 μm for all the images. (d) MoS_2-thickness histograms corresponding to the maps in (c). The peaks at 0 nm and ~0.7 nm correspond to the substrate and the monolayer MoS_2 (1L), respectively. Some small bilayer ~1.4 nm (2L) and trilayer ~2.1 nm (3L) regions are also observed in the sample on silica as shown in the inset.

in Fig. 3c. The bare-substrate spectra are reported as the dark-red lines, whereas the MoS_2-covered areas are reported as the green spectra. The differences between the spectra collected on different substrates are readily understandable based on the respective differences in dielectric function and morphology. In all the MoS_2-covered spectra, variations of different magnitudes with respect to the spectra on the bare substrate are observed, whose extent and spectral shape depended upon the dielectric mismatch of MoS_2 and the substrate material. The optical model parameters were optimized to best fit the experimental data, resulting in good agreement between models and data. The resulting fit curves are represented by dashed lines in Fig. 3b for each system.

Using these models, we performed pixel-by-pixel fitting of the iSE maps, leaving the MoS_2 thickness as the only free-fit parameter. The resulting thickness maps are shown in Fig. 3c, and the corresponding thickness histograms are displayed in Fig. 3d. The thickness maps clearly show that, beside some inhomogeneous areas, all the substrates under consideration feature large-area uniform monolayer MoS_2 regions, with lateral dimensions ranging from hundreds of microns to mm. Small bilayer, trilayer and bulk regions are present on the silica and PDMS substrates, but overall it is apparent that the method is able to produce large area monolayer MoS_2 samples on different substrates. iSE, besides confirming the monolayer nature of the exfoliated samples on millimetre-sized regions, allowed enhancement of the visibility compared to the optical images in Fig. 2 enhancing the contrast between the MoS_2 and the substrate on all the substrates. This is of particular interest for SiO_2(nat)/Si, PDMS and silica, where the flakes are invisible or barely visible.

Structural, chemical and photonic properties

Once we had ascertained the presence of large-area MoS_2 flakes, we proceeded to assess their structural, chemical and photonic characteristics, by means of X-ray photoemission spectroscopy (XPS), Raman spectroscopy and photoluminescence (PL).

Fig. 4a shows the XPS survey spectra of large-area MoS_2 over the four different substrates. The S/Mo ratio was extracted from the spectra in Fig. 4a obtaining a ratio of 1.9 ± 0.1 and 2.0 ± 0.1 for the samples on SiO_2(nat)/Si and SiO_2(285 nm)/Si, respectively (please see the SI for more details). All the spectra exhibit prominent Si, S, Mo, C, and O peaks originating from MoS_2 (Mo and S), the substrates (Si and O, and C in the case of PDMS) and adventitious contamination (C). Traces of iodine due to the etching solution can be found on the SiO_2(285 nm)/Si sample and on the PDMS sample. In particular, PDMS substrates undergoing the etching procedure turn slightly yellow after being in contact with the etchant, suggesting a reaction with PDMS that, however, does not alter its viscoelastic properties. The Si 2p peaks of the SiO_2(nat.)/Si sample are split into low-BE components (pure Si) and high-BE components (SiO_2).

Fig. 4b shows high resolution (HR) XPS spectra of the four samples, performed in the energy ranges corresponding to the Mo 3p/N 1s, Mo 3d/S 2s, S 2p, and C 1s peaks. The high-resolution spectra were deconvolved into their chemically shifted subcomponents as detailed in the Methods section. In general, the XPS spectra in corresponding energy regions share similar structures. The binding energies (BEs) of the Mo 3p, Mo 3d, N 1s, S 2s and S 2p peaks are all reported in Table 1. The binding energy was referenced to Mo $3d_{5/2}$ at 229.5 eV, since C 1s referencing is not appropriate for comparing data across these substrates.[54] From the deconvolution procedure, we can observe that the Mo $3d_{5/2}/3d_{3/2}$ peak is composed of a single doublet, unambiguously indicating that only the Mo(IV) states involved in MoS_2 are present, and justifying the energy referencing. The broad feature centred around 416 eV BE (hatched area) can be attributed to plasmon losses. Similarly, the absence of further components near the S $2p_{3/2}/2p_{1/2}$ doublet confirms that sulphur is not involved in chemical bonds other than MoS_2. The larger FWHM of the peaks (especially the S 2p) for the PDMS sample is ascribed to the superposition of contributions from monolayer and few-layer areas, given that the XPS measuring spot has a few hundred microns of lateral dimension. The N 1s peak around 399 eV BE verifies the presence of very small quantities of nitrogen that can, however, be observed in the bare substrates. Fig. S6 shows the XPS survey spectrum of each substrate prior to the deposition of MoS_2.

Raman and PL measurements can be exploited to gain insights into the presence of defects,[55,56] strain[57,58] and doping[59–61] in monolayer flakes. Fig. 5 shows representative Raman and PL spectra of the samples on each substrate. The in-plane E^1_{2g} and the out-of-plane A_{1g} Raman mode frequencies are compatible with the typical values found in the literature. The frequency difference between the two modes was found at values ranging from $\sim$18.6 cm^{-1} to $\sim$19.5 cm^{-1} for all the samples, fully compatible with monolayer MoS_2 samples. PL spectra, reported in Fig. 5b, show clear differences depending on the target substrates, in particular with regard to the relative spectral weights of neutral exciton, trion and B-exciton contributions. When looking at the A^0 exciton ($\sim$1.9 eV) and the A^- trion ($\sim$1.85 eV), we observe a strong variation of the peak intensity ratio $I(A^-)/I(A^0)$ among the samples. Fig. 5c shows the mean value and deviation of the neutral-exciton/trion ratio for each substrate, with each measurement resulting from the average of over 500 points (the full distribution of the parameters is shown in Fig. S7). We can easily notice that the PDMS sample features a substantially lower $I(A^-)/I(A^0)$ ratio when compared to the other samples, a difference compatible either with the presence of defects or with low substrate-induced doping. In the case that defects gave the larger contribution, however, the intensity ratio of the A and B excitons $I(B)/I(A^0)$ should also increase,[55] but the data show that the B exciton intensity on PDMS is very weak compared to that of the A exciton, resulting in the low $I(B)/I(A^0)$ ratio observed in Fig. 5c. As a consequence, the difference between the PL spectra of the PDMS sample and the other ones can be assigned to a lower substrate-induced doping of MoS_2 in the PDMS case. In contrast, the higher $I(A^-)/I(A^0)$ ratios observed in all the remaining samples indicate higher electron doping levels, as indeed observed in MoS_2 samples deposited on silicon oxide

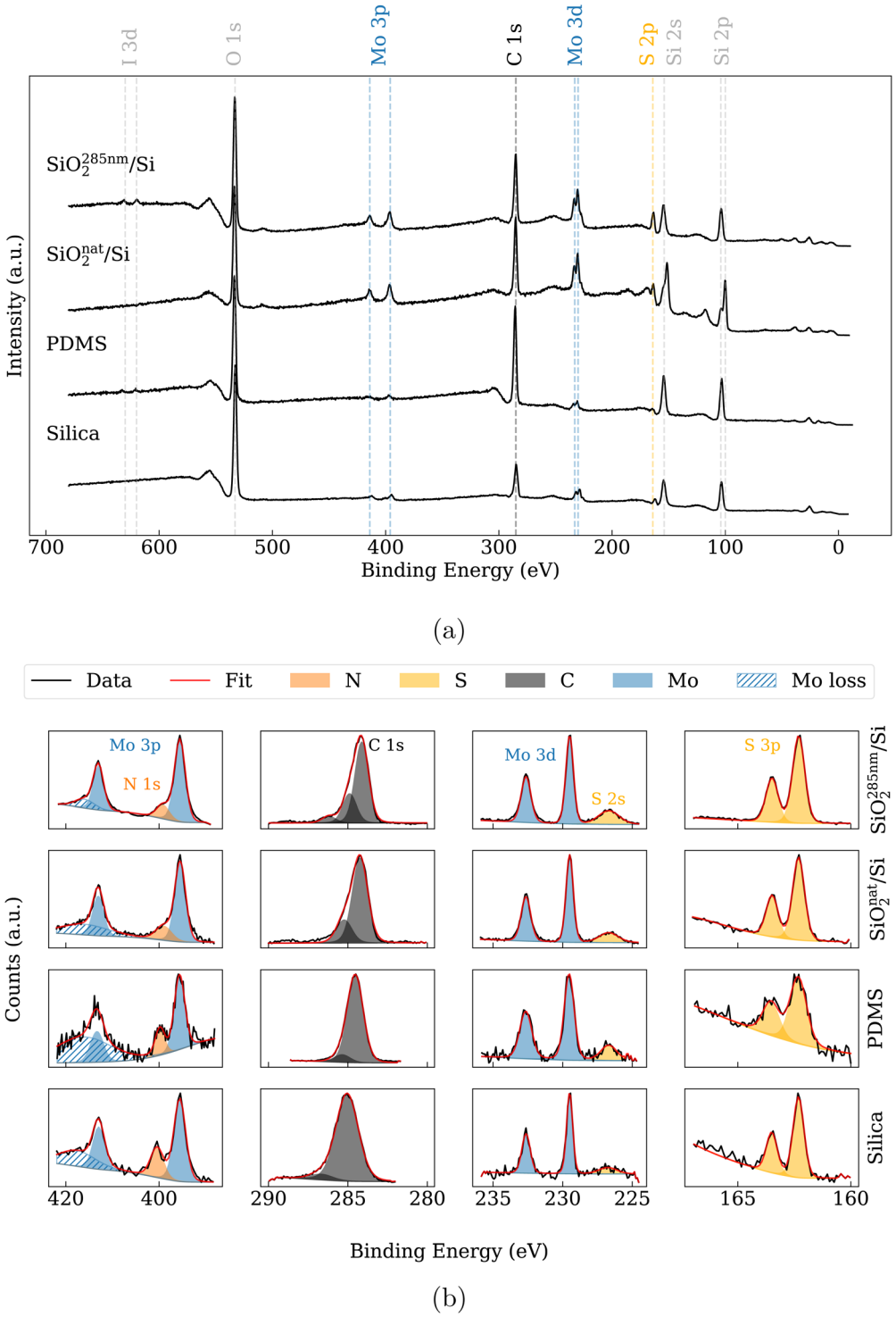

Fig. 4 (a) XPS survey spectra of the samples on the different substrates. Vertical dashed lines have been added as a guide to the eye for tracing the major XPS peaks present in the spectra. (b) High-resolution measurements performed in the Mo 3d, Mo 3p, N 1s, C 1s and S 2p energy regions. Each row corresponds to a different substrate labelled on the right side of the figure.

surfaces.[62–67] Detailed characterization of the substrate induced doping effect was beyond the scope of this work.

Finally, we notice that both PL and Raman spectra of native-oxide Si exhibit lower signals compared to other samples, despite being acquired under analogous experimental conditions. Since both Raman and PL spectra do not significantly differ from those of MoS_2 on silica or thermal-oxide Si, we suggest that such a reduced signal might originate from dielectric screening and charge transfer effects between MoS_2 and the underlying Si. While, to our knowledge, there are no studies that directly involve PL and Raman measurements of MoS_2 on Si substrates, our hypothesis is supported by several

Table 1 Binding energies of the main XPS peaks

Substrate	S $2p_{3/2}$	S $2p_{1/2}$	S 2s	Mo $3d_{5/2}$	Mo $3d_{3/2}$	Mo $3p_{3/2}$	Mo $3p_{1/2}$	N 1s
SiO_2(nat)/Si	162.3	163.5	226.7	229.5	232.6	395.5	413.1	399.0
SiO_2(285 nm)/Si	162.3	163.5	226.7	229.5	232.6	395.5	413.0	399.2
PDMS	162.3	163.5	226.7	229.5	232.7	395.6	413.3	399.8
Silica	162.3	163.5	226.8	229.5	232.6	395.6	413.0	400.4

studies of TMDCs on semiconducting and metallic surfaces[30,68–71] showing the quenching of the MoS_2 PL due to charge transfer and dielectric screening effects.

Deterministic transfer from PDMS stamps

The successful exfoliation of large-area flakes on PDMS opens up interesting perspectives, since PDMS is widely employed as a vector for the deterministic transfer of TMDC flakes onto a large variety of substrates.[42,43] It would, therefore, be extremely appealing to replicate such procedures with the very large flakes that we fabricate, thereby extending the range of possible target substrates to systems not currently compatible with the above-reported exfoliation technique, like noble-metal films. Furthermore, several applications of TMDCs, such as vdW heterostructures for electronics or optoelectronics, require deterministic transfer approaches, which are intrinsically not guaranteed by the exfoliation process alone. In this section, we demonstrate the deterministic transfer of MoS_2 on a given substrate, adapting a common all dry-transfer method,[42] performing a successful transfer on SiO_2(nat)/Si of our sample exfoliated on PDMS (Fig. 2c).

In Fig. 6, we show a binary intensity map of the sample before and after the transfer, constructed by identifying the MoS_2 regions in the corresponding optical images (Fig. S8). We can observe that the original sample (Fig. 6a) is almost entirely transferred onto the target substrate (Fig. 6b). Partial fragmentation is observed in the localized region of the sample; however, large uniform areas are still present after the sample is transferred.

The sample was then characterized by Raman and PL spectroscopy in order to assess its properties after the transfer. In Fig. 7, we compare the spectra acquired before and after performing the transfer. We can observe that the spectroscopic features of MoS_2 are hardly affected by the sample transfer. We observe, however, a significant reduction in both the Raman and PL intensities after the transfer, comparable to what is observed with the sample directly produced on SiO_2(nat)/Si in Fig. 2b. With a similar argument to that provided in the previous section, we can trace back this quenching effect to the interaction of the MoS_2 sample with the underlying silicon substrate, rather than being an intrinsic feature of the transferred MoS_2. Finally, we observe that the transferred sample features a lower $I(A^-)/I(A^0)$ ratio compared to the one observed using the same substrate in Fig. 5b. This can indicate that the interaction between the substrate and MoS_2 is partially reduced

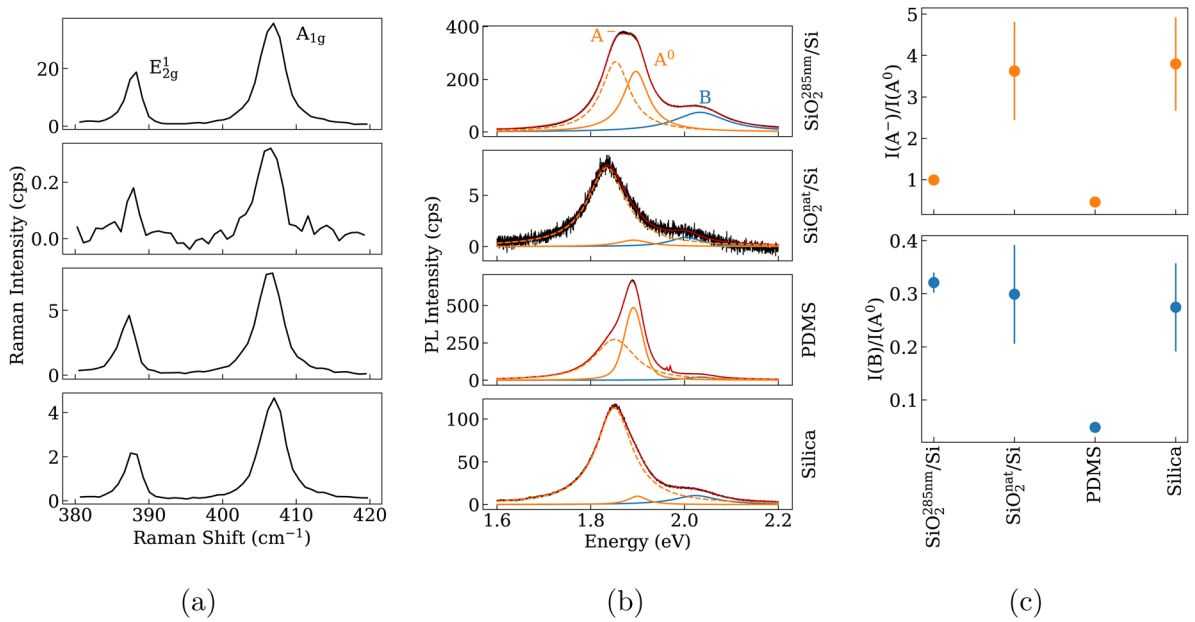

Fig. 5 (a) Raman and (b) photoluminescence spectra. The black line shows the background-subtracted experimental data. In the PL plots, the orange solid and dashed lines and the blue solid line indicate the fitted A^0 exciton, A^- trion and B exciton peaks, respectively. The solid red line shows the complete fitting function. (c) $I(B)/I(A^0)$ (bottom) and $I(A^-)/I(A^0)$ (top) intensity ratios extracted from the distributions in Fig. S7.

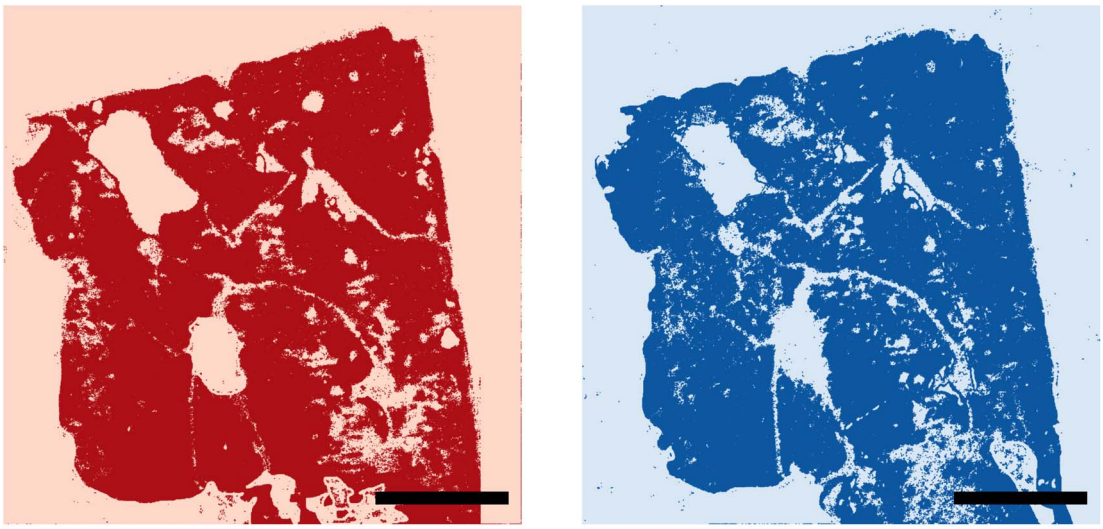

Fig. 6 Binary maps extracted from the optical images in Fig. S8 of the sample exfoliated on PDMS before (a) and after (b) its transfer on a SiO_2(nat)/Si substrate. The darker colours in both images correspond to areas identified as MoS_2. The scale bar is 250 μm.

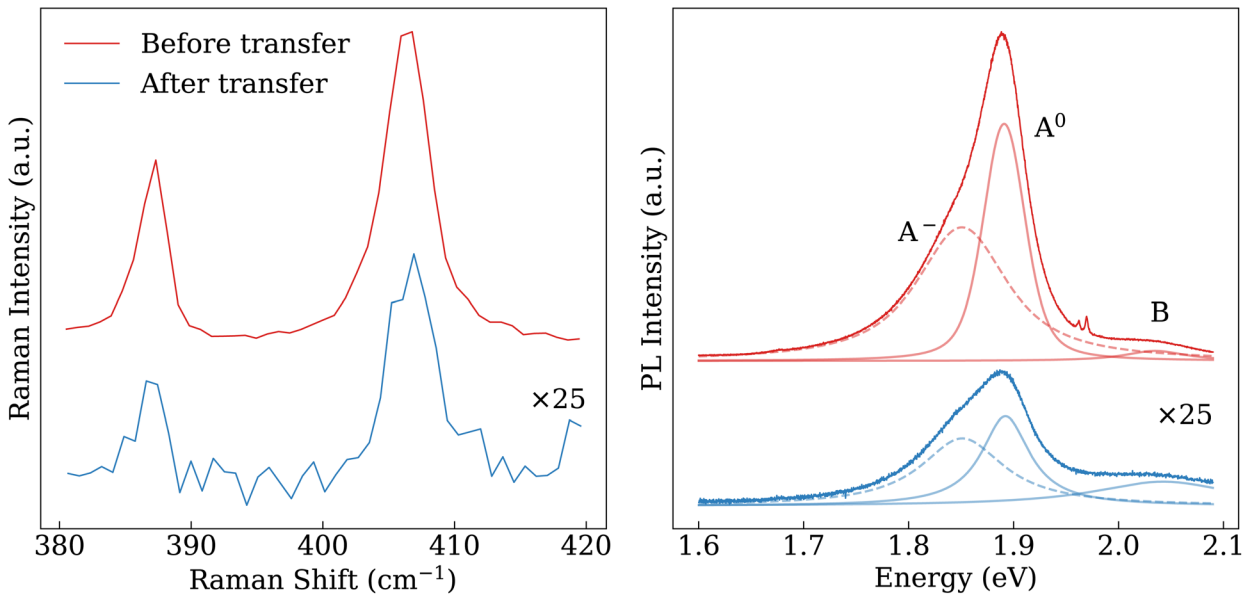

Fig. 7 Characteristic Raman (left) and PL (right) spectra of the transferred sample before and after the transfer. The intensity of the spectra of the transferred sample was multiplied by a factor 25.

due to contaminants associated with the PDMS transfer procedure.[52,72]

Several other transfer attempts were performed on different substrates, to demonstrate the potential of combining our large-area exfoliation method with the PDMS dry-transfer technique. In the SI, we report two representative cases of flakes transferred onto noteworthy substrates such as Si_3N_4 ultra-thin membrane used for TEM measurement (Fig. S9) and optical microcavities nanofabricated on a silver film on CaF_2 (Fig. S10).

Conclusions

In the present work, we report a groundbreaking improvement of the previously reported gold-assisted mechanical exfoliation of bulk MoS_2. This method allowed the production of millimeter-sized flakes on four different substrates, representative of various applications in electronics and optoelectronics. In particular, the modification of one of the exfoliation steps, introducing a PDMS layer mechanically constraining the TRT during the release phase, allowed an increase in the reliability of the exfoliation and enabled its generalization to different

substrates. The key advantages of our method are its simplicity, scalability, reliability, cost-effectiveness and quickness. Uniquely, the exfoliation can be performed on a wide range of target substrates without modifying the exfoliation procedure. Notably, the gold-assisted exfoliation of large MoS_2 samples on PDMS has been demonstrated. PDMS is a resourceful substrate material that enabled us to perform further deterministic transfers of the freshly exfoliated, millimeter-sized samples onto desired substrates with micrometric control over the positioning of the 2D material.

Imaging ellipsometry has been employed to assess the local MoS_2 thickness over large areas, thus enabling a fast and reliable determination of the monolayer nature of our exfoliated flakes. Moreover, our samples were characterized by Raman and photoluminescence spectroscopy in order to grade the quality and uniformity of the exfoliated samples. We observed substrate-dependent variations of the spectral features of the MoS_2 samples, which were identified as due to substrate–MoS_2 interactions. Overall, a high photoluminescence yield is observed, indicating high-quality monolayer samples. A Raman and photoluminescence quenching effect for the sample on SiO_2(nat)/Si was traced back to substrate/MoS_2 interactions, as well as intensity and PL peak shifts between different substrates.

The presented methodology represents a major breakthrough in the production of 2D materials. We believe that its flexibility and scalability will drive major advancements in the fabrication of macroscopic 2D devices, ultimately enabling the complete exploitation of the exceptional properties of 2D materials.

Methods

Imaging Spectroscopic Ellipsometry (iSE) measurements were performed by means of a Park Systems Accurion EP4 imaging ellipsometer equipped with a laser-stabilized Xenon lamp and a monochromator. We acquired all our spectra in the 360 nm to 1000 nm range at an angle of incidence of 50° in rotating compensator mode. A 5× objective was used to focus the collected light to a CCD detector, simultaneously acquiring the whole probed area. Knife-edge illumination was used to block backside reflections and accurately measure the ellipsometric quantities on double-polished transparent substrates (PDMS and silica).

XPS spectra were acquired using a Physical Electronics PHI 5600 photoelectron spectrometer, equipped with a monochromatized Al K_α source and with an electron flood gun to reduce surface charging. XPS data analysis was performed using CasaXPS software. The spectra were fitted using the symmetric Voigt-like LA(1.53, 243) line shape in CasaXPS. The S 2p, Mo 3p, and Mo 3d doublets were fitted while keeping the $p_{3/2}$:$p_{1/2}$ and $d_{5/2}$:$d_{3/2}$ area ratios fixed at 2 : 1 and 3 : 2, respectively. The S 2p spin-orbit peaks were also constrained to have the same full-width at half-maximum (FWHM). The Mo 3p and Mo 3d spin-orbit peaks were allowed to have different FHWMs to better reproduce the experimental data. The need for a non-identical FWHM to fit the Mo doublets is due to Coster–Kronig broadening, which has been observed on similar compounds.[73–75] The C 1s peak has been fitted with two components with the same FWHM, except for the sample on SiO_2(285 nm)/Si, where the spectral lineshape clearly suggests a third component at higher binding energies, which can be attributed to additional contamination.

Micro-Raman and photoluminescence spectroscopy were performed using a Jasco NRS-4100 Raman spectrometer. The probing laser was a 532 nm laser filtered to have a power of ~100 μW on the sample through a 100×, 0.9 NA objective. A 2400 grooves/mm grating was used to disperse scattered light for the Raman measurements; a 900 grooves/mm grating was used for photoluminescence measurements.

Conflicts of interest

There are no conflicts to declare.

Data availability

The datasets analysed during the current study are available at https://doi.org/10.5281/zenodo.17602072.

Supplementary information (SI): (S1) photos of the exfoliation steps; (S2) samples of Δ values acquired with the imaging ellipsometer; (S3) samples of Ψ values acquired with the imaging ellipsometer; (S4) AFM imaging of a sample on SiO_2(nat)/Si; (S5) graphical representation of the models used for the fitting of the ellipsometric quantities Ψ and Δ; (S6) XPS quantitative analysis; (S7) distributions of I(B)/I(A^0) and I(A^-)/I(A^0) from PL mapping; (S8) optical images of the MoS_2 sample on PDMS before and after performing its transfer onto a SiO_2(nat)/Si substrate; (S9) optical images of the transfer of a MoS_2 monolayer onto a Si_3N_4 TEM grid; (S10) optical images of the transfer onto a silver-coated, nanofabricated CaF_2 substrate; tabulated optical constants of monolayer MoS_2. See DOI: https://doi.org/10.1039/d5na00919g.

Acknowledgements

We thank doctor N. Petrini and professor I. Kriegel for the critical reading of the manuscript. This work was carried out within the framework of the project "RAISE – Robotics and AI for Socio–economic Empowerment" and has been supported by European Union – NextGenerationEU. Funded by the European Union – NextGenerationEU. However, the views and opinions expressed are those of the authors alone and do not necessarily reflect those of the European Union or the European Commission. Neither the European Union nor the European Commission can be held responsible for them. Authors acknowledge financial support under the National Recovery and Resilience Plan (NRRP), Mission 4, Component 2, Investment 1.1, Call for tender no. 104 PRIN 2022 published on 2.2.2022 by the Italian Ministry of University and Research (MUR), funded by the European Union – NextGenerationEU – Project Title ERACLITO – CUP B53D2300904006 and Call for tender no. 1409 PRIN PNRR 2022 published on 14.9.2022 by the Italian Ministry of University and Research (MUR), funded by the European Union

– NextGenerationEU – Project Title ARCO – CUP B53D23027690001.

References

1 K. S. Novoselov, A. K. Geim, S. V. Morozov, D. Jiang, Y. Zhang, S. V. Dubonos, I. V. Grigorieva and A. A. Firsov, Electric Field Effect in Atomically Thin Carbon Films, *Science*, 2004, **306**, 666–669.

2 K. S. Novoselov, A. Mishchenko, A. Carvalho and A. H. C. Neto, 2D materials and van der Waals heterostructures, *Science*, 2016, **353**, aac9439.

3 S. Manzeli, D. Ovchinnikov, D. Pasquier, O. V. Yazyev and A. Kis, 2D transition metal dichalcogenides, *Nat. Rev. Mater.*, 2017, **2**, 1–15.

4 A. Splendiani, L. Sun, Y. Zhang, T. Li, J. Kim, C.-Y. Chim, G. Galli and F. Wang, Emerging Photoluminescence in Monolayer MoS_2, *Nano Lett.*, 2010, **10**, 1271–1275.

5 A. Chernikov, T. C. Berkelbach, H. M. Hill, A. Rigosi, Y. Li, B. Aslan, D. R. Reichman, M. S. Hybertsen and T. F. Heinz, Exciton Binding Energy and Nonhydrogenic Rydberg Series in Monolayer WS_2, *Phys. Rev. Lett.*, 2014, **113**, 076802.

6 K. F. Mak, K. He, J. Shan and T. F. Heinz, Control of valley polarization in monolayer MoS_2 by optical helicity, *Nat. Nanotechnol.*, 2012, **7**, 494–498.

7 D. Jariwala, V. K. Sangwan, L. J. Lauhon, T. J. Marks and M. C. Hersam, Emerging Device Applications for Semiconducting Two-Dimensional Transition Metal Dichalcogenides, *ACS Nano*, 2014, **8**, 1102–1120.

8 G. Wang, A. Chernikov, M. M. Glazov, T. F. Heinz, X. Marie, T. Amand and B. Urbaszek, Colloquium: Excitons in atomically thin transition metal dichalcogenides, *Rev. Mod. Phys.*, 2018, **90**, 021001.

9 A. Raza, J. Z. Hassan, M. Ikram, S. Ali, U. Farooq, Q. Khan and M. Maqbool, Advances in Liquid-Phase and Intercalation Exfoliations of Transition Metal Dichalcogenides to Produce 2D Framework, *Adv. Mater. Interfaces*, 2021, **8**, 2002205.

10 Y.-H. Lee, X.-Q. Zhang, W. Zhang, M.-T. Chang, C.-T. Lin, K.-D. Chang, Y.-C. Yu, J. T.-W. Wang, C.-S. Chang, L.-J. Li and T.-W. Lin, Synthesis of Large-Area MoS_2 Atomic Layers with Chemical Vapor Deposition, *Adv. Mater.*, 2012, **24**, 2320–2325.

11 Q. Wang, *et al.*, Wafer-Scale Highly Oriented Monolayer MoS_2 with Large Domain Sizes, *Nano Lett.*, 2020, **20**, 7193–7199.

12 M. Chubarov, T. H. Choudhury, D. R. Hickey, S. Bachu, T. Zhang, A. Sebastian, A. Bansal, H. Zhu, N. Trainor, S. Das, M. Terrones, N. Alem and J. M. Redwing, Wafer-Scale Epitaxial Growth of Unidirectional WS_2 Monolayers on Sapphire, *ACS Nano*, 2021, **15**, 2532–2541.

13 P. Yang, *et al.*, Epitaxial Growth of Centimeter-Scale Single-Crystal MoS_2 Monolayer on Au(111), *ACS Nano*, 2020, **14**, 5036–5045.

14 H. Jiang, X. Zhang, K. Chen, X. He, Y. Liu, H. Yu, L. Gao, M. Hong, Y. Wang, Z. Zhang and Y. Zhang, Two-dimensional Czochralski growth of single-crystal MoS_2, *Nat. Mater.*, 2025, **24**, 188–196.

15 M. Velický, *et al.*, Mechanism of Gold-Assisted Exfoliation of Centimeter-Sized Transition-Metal Dichalcogenide Monolayers, *ACS Nano*, 2018, **12**, 10463–10472.

16 G. Z. Magda, J. Pető, G. Dobrik, C. Hwang, L. P. Biró and L. Tapasztó, Exfoliation of large-area transition metal chalcogenide single layers, *Sci. Rep.*, 2015, **5**, 14714.

17 S. B. Desai, S. R. Madhvapathy, M. Amani, D. Kiriya, M. Hettick, M. Tosun, Y. Zhou, M. Dubey, J. W. Ager, D. Chrzan and A. Javey, Gold-mediated exfoliation of ultralarge optoelectronically-perfect monolayers, *Adv. Mater.*, 2016, **28**, 4053–4058.

18 F. Liu, Mechanical exfoliation of large area 2D materials from vdW crystals, *Prog. Surf. Sci.*, 2021, **96**, 100626.

19 M. Heyl and E. J. List-Kratochvil, Only gold can pull this off: mechanical exfoliations of transition metal dichalcogenides beyond scotch tape, *Appl. Phys. A*, 2023, **129**, 16.

20 S. E. Panasci, E. Schilirò, F. Roccaforte and F. Giannazzo, Gold-Assisted Exfoliation of Large-Area Monolayer Transition Metal Dichalcogenides: From Interface Properties to Device Applications, *Adv. Funct. Mater.*, 2025, **35**, 2414532.

21 S. Sahu, G. Haider, A. Rodriguez, J. Plšek, M. Mergl, M. Kalbáč, O. Frank and M. Velický, Large-Area Mechanically-Exfoliated Two-Dimensional Materials on Arbitrary Substrates, *Adv. Mater. Technol.*, 2023, **8**, 2201993.

22 N. Olsen, *et al.*, Macroscopic Transition Metal Dichalcogenide Monolayers from Gold-Tape Exfoliation Retain Intrinsic Properties, *Nano Lett.*, 2025, **25**, 15198–15205.

23 M. Heyl, D. Burmeister, T. Schultz, S. Pallasch, G. Ligorio, N. Koch and E. J. W. List-Kratochvil, Thermally Activated Gold-Mediated Transition Metal Dichalcogenide Exfoliation and a Unique Gold-Mediated Transfer, *Phys. Status Solidi RRL*, 2020, **14**, 2000408.

24 L. Pirker, J. Honolka, M. Velický and O. Frank, When 2D materials meet metals, *2D Mater.*, 2024, **11**, 022003.

25 Y. Huang, *et al.*, Universal mechanical exfoliation of large-area 2D crystals, *Nat. Commun.*, 2020, **11**, 2453.

26 X. Huang, L. Zhang, L. Liu, Y. Qin, Q. Fu, Q. Wu, R. Yang, J.-P. Lv, Z. Ni, L. Liu, W. Ji, Y. Wang, X. Zhou and Y. Huang, Raman spectra evidence for the covalent-like quasi-bonding between exfoliated MoS_2 and Au films, *Sci. China Inf. Sci.*, 2021, **64**, 140406.

27 M. Hanušová, *et al.*, Hybridization Directionality Governs the Interaction Strength between MoS_2 and Metals, *Nano Lett.*, 2025, **25**, 12995–13002.

28 M. Farmanbar and G. Brocks, First-principles study of van der Waals interactions and lattice mismatch at MoS_2/metal interfaces, *Phys. Rev. B*, 2016, **93**, 085304.

29 M. Velický, A. Rodriguez, M. Bouša, A. V. Krayev, M. Vondráček, J. Honolka, M. Ahmadi, G. E. Donnelly, F. Huang, H. D. Abruña, K. S. Novoselov and O. Frank, Strain and Charge Doping Fingerprints of the Strong Interaction between Monolayer MoS_2 and Gold, *J. Phys. Chem. Lett.*, 2020, **11**, 6112–6118.

30 E. Pollmann, S. Sleziona, T. Foller, U. Hagemann, C. Gorynski, O. Petri, L. Madauß, L. Breuer and M. Schleberger, Large-Area, Two-Dimensional MoS_2 Exfoliated on Gold: Direct Experimental Access to the Metal–Semiconductor Interface, *ACS Omega*, 2021, **6**, 15929–15939.
31 S. E. Panasci, E. Schilirò, G. Greco, M. Cannas, F. M. Gelardi, S. Agnello, F. Roccaforte and F. Giannazzo, Strain, Doping, and Electronic Transport of Large Area Monolayer MoS_2 Exfoliated on Gold and Transferred to an Insulating Substrate, *ACS Appl. Mater. Interfaces*, 2021, **13**, 31248–31259.
32 A. Rodriguez, M. c. v. Velický, J. Řáhová, V. Zólyomi, J. Koltai, M. Kalbáč and O. Frank, Activation of Raman modes in monolayer transition metal dichalcogenides through strong interaction with gold, *Phys. Rev. B*, 2022, **105**, 195413.
33 H. Sun, E. W. Sirott, J. Mastandrea, H. M. Gramling, Y. Zhou, M. Poschmann, H. K. Taylor, J. W. Ager and D. C. Chrzan, Theory of thin-film-mediated exfoliation of van der Waals bonded layered materials, *Phys. Rev. Mater.*, 2018, **2**, 094004.
34 J. Ziewer, A. Ghosh, M. Hanušová, L. Pirker, O. Frank, M. Velický, M. Grüning and F. Huang, Strain-Induced Decoupling Drives Gold-Assisted Exfoliation of Large-Area Monolayer 2D Crystals, *Adv. Mater.*, 2025, **37**, 2419184.
35 A. Corletto, M. Fronzi, A. K. Joannidis, P. C. Sherrell, M. J. Ford, D. A. Winkler, J. G. Shapter, J. Bullock and A. V. Ellis, A Predictive Model for Monolayer-Selective Metal-Mediated MoS_2 Exfoliation Incorporating Electrostatics, *Adv. Mater. Interfaces*, 2024, **11**, 2300686.
36 A. C. Johnston and S. I. Khondaker, Can Metals Other than Au be Used for Large Area Exfoliation of MoS_2 Monolayers?, *Adv. Mater. Interfaces*, 2022, **9**, 2200106.
37 M. Velický, G. E. Donnelly, W. R. Hendren, W. J. I. DeBenedetti, M. A. Hines, K. S. Novoselov, H. D. Abruña, F. Huang and O. Frank, The Intricate Love Affairs between MoS_2 and Metallic Substrates, *Adv. Mater. Interfaces*, 2020, **7**, 2001324.
38 S. Ding, *et al.*, Ag-Assisted Dry Exfoliation of Large-Scale and Continuous 2D Monolayers, *ACS Nano*, 2024, **18**, 1195–1203.
39 F. Liu, W. Wu, Y. Bai, S. H. Chae, Q. Li, J. Wang, J. Hone and X.-Y. Zhu, Disassembling 2D van der Waals crystals into macroscopic monolayers and reassembling into artificial lattices, *Science*, 2020, **367**, 903–906.
40 N. Petrini, E. Peci, N. Curreli, E. Spotorno, N. Kazemi Tofighi, M. Magnozzi, F. Scotognella, F. Bisio and I. Kriegel, Optimizing Gold-Assisted Exfoliation of Layered Transition Metal Dichalcogenides with (3-Aminopropyl) triethoxysilane (APTES): A Promising Approach for Large-Area Monolayers, *Adv. Opt. Mater.*, 2024, **12**, 2303228.
41 L. Ramò, E. Peci, M. Magnozzi, E. Spotorno, V. Venturino, M. Sygletou, M. C. Giordano, G. Zambito, F. Telesio, Z. Milosz, M. Canepa and F. Bisio, Noninvasive Deterministic Nanostructures Lithography on 2D Transition Metal Dichalcogenides, *Adv. Eng. Mater.*, 2025, **27**, 2401157.
42 A. Castellanos-Gomez, M. Buscema, R. Molenaar, V. Singh, L. Janssen, H. S. J. van der Zant and G. A. Steele, Deterministic transfer of two-dimensional materials by all-dry viscoelastic stamping, *2D Mater.*, 2014, **1**, 011002.
43 A. J. Watson, W. Lu, M. H. D. Guimarães and M. Stöhr, Transfer of large-scale two-dimensional semiconductors: challenges and developments, *2D Mater.*, 2021, **8**, 032001.
44 M. Velický, *et al.*, Mechanism of Gold-Assisted Exfoliation of Centimeter-Sized Transition-Metal Dichalcogenide Monolayers, *ACS Nano*, 2018, **12**, 10463–10472.
45 Q. Fu, *et al.*, One-Step Exfoliation Method for Plasmonic Activation of Large-Area 2D Crystals, *Adv. Sci.*, 2022, **9**, 2204247.
46 G. Haider, M. Gastaldo, B. Karim, J. Plšek, V. Varade, O. Volochanskyi, J. Vejpravová and M. Kalbáč, Highly Efficient Bulk-Crystal-Sized Exfoliation of 2D Materials under Ultrahigh Vacuum, *ACS Appl. Electron. Mater.*, 2024, **6**, 2301–2308.
47 M. Magnozzi, T. Pflug, M. Ferrera, S. Pace, L. Ramó, M. Olbrich, P. Canepa, H. Ağircan, A. Horn, S. Forti, O. Cavalleri, C. Coletti, F. Bisio and M. Canepa, Local Optical Properties in CVD-Grown Monolayer WS_2 Flakes, *J. Phys. Chem. C*, 2021, **125**, 16059–16065.
48 M. Magnozzi, M. Ferrera, G. Piccinini, S. Pace, S. Forti, F. Fabbri, C. Coletti, F. Bisio and M. Canepa, Optical dielectric function of two-dimensional WS_2 on epitaxial graphene, *2D Mater.*, 2020, **7**, 025024.
49 S. Funke, B. Miller, E. Parzinger, P. Thiesen, A. W. Holleitner and U. Wurstbauer, Imaging spectroscopic ellipsometry of MoS_2, *J. Phys. Condens. Matter*, 2016, **28**, 385301.
50 E. Peci, N. Petrini, N. Curreli, E. Spotorno, N. K. Tofighi, M. Magnozzi, F. Scotognella, I. Kriegel and F. Bisio, Fast thickness mapping of large-area exfoliated two-dimensional transition metal dichalcogenides by imaging spectroscopic ellipsometry, *EPJ Web Conf.*, 2024, **309**, 06006.
51 C. J. Shearer, A. D. Slattery, A. J. Stapleton, J. G. Shapter and C. T. Gibson, Accurate thickness measurement of graphene, *Nanotechnology*, 2016, **27**, 125704.
52 Y. Pan and D. R. T. Zahn, Raman Fingerprint of Interlayer Coupling in 2D TMDCs, *Nanomaterials*, 2022, **12**(22), 3949.
53 E. Peci, M. Magnozzi, L. Ramò, M. Ferrera, D. Convertino, S. Pace, G. Orlandini, A. Sharma, I. Milekhin, G. Salvan, C. Coletti, D. R. T. Zahn, F. Bisio and M. Canepa, Dielectric Function of 2D Tungsten Disulfide in Homo- and Heterobilayer Stacking, *Adv. Mater. Interfaces*, 2023, **10**, 2201586.
54 G. Greczynski and L. Hultman, Binding energy referencing in X-ray photoelectron spectroscopy, *Nat. Rev. Mat.*, 2025, **10**, 62–78.
55 K. M. McCreary, A. T. Hanbicki, S. V. Sivaram and B. T. Jonker, A- and B-exciton photoluminescence intensity ratio as a measure of sample quality for transition metal dichalcogenide monolayers, *APL Mater.*, 2018, **6**, 111106.
56 F. B. Sousa, R. Nadas, R. Martins, A. P. M. Barboza, J. S. Soares, B. R. A. Neves, I. Silvestre, A. Jorio and L. M. Malard, Disentangling doping and strain effects at defects of grown MoS_2 monolayers with nano-optical spectroscopy, *Nanoscale*, 2024, **16**, 12923–12933.

57 Z. Liu, *et al.*, Strain and structure heterogeneity in MoS_2 atomic layers grown by chemical vapour deposition, *Nat. Commun.*, 2014, **5**, 5246.
58 A. Castellanos-Gomez, R. Roldán, E. Cappelluti, M. Buscema, F. Guinea, H. S. J. van der Zant and G. A. Steele, Local Strain Engineering in Atomically Thin MoS_2, *Nano Lett.*, 2013, **13**, 5361–5366.
59 D. Vaquero, V. Clericò, J. Salvador-Sánchez, A. Martín-Ramos, E. Díaz, F. Domínguez-Adame, Y. M. Meziani, E. Diez and J. Quereda, Excitons, trions and Rydberg states in monolayer MoS_2 revealed by low-temperature photocurrent spectroscopy, *Commun. Phys.*, 2020, **3**, 194.
60 S. Mouri, Y. Miyauchi and K. Matsuda, Tunable Photoluminescence of Monolayer MoS_2 *via* Chemical Doping, *Nano Lett.*, 2013, **13**, 5944–5948.
61 E. Peci, Y. Pan, E. Spotorno, L. Ramò, F. Telesio, M. Magnozzi, Z. Miłosz, L. Gregoratti, M. Amati, N. Petrini, I. Kriegel, D. R. T. Zahn, M. Canepa and F. Bisio, Laser-Induced Sulfur Vacancy Defect Healing by Oxygen in Molybdenum Disulfide Monolayers, *J. Phys. Chem. C*, 2025, **129**, 21407–21417.
62 N. Scheuschner, O. Ochedowski, A.-M. Kaulitz, R. Gillen, M. Schleberger and J. Maultzsch, Photoluminescence of freestanding single- and few-layer MoS_2, *Phys. Rev. B:Condens. Matter Mater. Phys.*, 2014, **89**, 125406.
63 M. Buscema, G. A. Steele, H. S. J. van der Zant and A. Castellanos-Gomez, The effect of the substrate on the Raman and photoluminescence emission of single-layer MoS_2, *Nano Res.*, 2014, **7**, 561–571.
64 W. H. Chae, J. D. Cain, E. D. Hanson, A. A. Murthy and V. P. Dravid, Substrate-induced strain and charge doping in CVD-grown monolayer MoS_2, *Appl. Phys. Lett.*, 2017, **111**, 143106.
65 X. Fan, R. Nouchi and K. Tanigaki, Effect of Charge Puddles and Ripples on the Chemical Reactivity of Single Layer Graphene Supported by SiO_2/Si Substrate, *J. Phys. Chem. C*, 2011, **115**, 12960–12964.
66 E. Ji, M. J. Kim, J.-Y. Lee, D. Sung, N. Kim, J.-W. Park, S. Hong and G.-H. Lee, Substrate effect on doping and degradation of graphene, *Carbon*, 2021, **184**, 651–658.
67 Y. Sun, R. Wang and K. Liu, Substrate induced changes in atomically thin 2-dimensional semiconductors: Fundamentals, engineering, and applications, *Appl. Phys. Rev.*, 2017, **4**, 011301.
68 R. R. Rojas-Lopez, J. C. Brant, M. S. O. Ramos, T. H. L. G. Castro, M. H. D. Guimarães, B. R. A. Neves and P. S. S. Guimarães, Photoluminescence and charge transfer in the prototypical 2D/3D semiconductor heterostructure MoS_2/GaAs, *Appl. Phys. Lett.*, 2021, **119**, 233101.
69 S. E. Panasci, E. Schilirò, F. Migliore, M. Cannas, F. M. Gelardi, F. Roccaforte, F. Giannazzo and S. Agnello, Substrate impact on the thickness dependence of vibrational and optical properties of large area MoS_2 produced by gold-assisted exfoliation, *Appl. Phys. Lett.*, 2021, **119**, 093103.
70 U. Bhanu, M. R. Islam, L. Tetard and S. I. Khondaker, Photoluminescence quenching in gold - MoS_2 hybrid nanoflakes, *Sci. Rep.*, 2014, **4**, 5575.
71 M. T. Hossain, L. P. L. Mawlong, T. Jena, A. Bora, U. Nath, M. Sarma and P. K. Giri, Interlayer Charge-Transfer-Induced Photoluminescence Quenching and Enhanced Photoconduction in Two-Dimensional Bi_2O_2Se/MoS_2 Type-II Heterojunction, *ACS Appl. Nano Mater.*, 2023, **6**, 11023–11036.
72 S. J. Haigh, A. Gholinia, R. Jalil, S. Romani, L. Britnell, D. C. Elias, K. S. Novoselov, L. A. Ponomarenko, A. K. Geim and R. Gorbachev, Cross-sectional imaging of individual layers and buried interfaces of graphene-based heterostructures and superlattices, *Nat. Mater.*, 2012, **11**, 764–767.
73 E. Nolot, S. Cadot, F. Martin, P. Hönicke, C. Zech and B. Beckhoff, In-line characterization of ultrathin transition metal dichalcogenides using X-ray fluorescence and X-ray photoelectron spectroscopy, *Spectrochim. Acta, Part B*, 2020, **166**, 105788.
74 L. A. H. Jones, Z. Xing, J. E. N. Swallow, H. Shiel, T. J. Featherstone, M. J. Smiles, N. Fleck, P. K. Thakur, T.-L. Lee, L. J. Hardwick, D. O. Scanlon, A. Regoutz, T. D. Veal and V. R. Dhanak, Band Alignments, Electronic Structure, and Core-Level Spectra of Bulk Molybdenum Dichalcogenides (MoS_2, $MoSe_2$, and $MoTe_2$), *J. Phys. Chem. C*, 2022, **126**, 21022–21033.
75 N. Mårtensson and R. Nyholm, Electron spectroscopic determinations of M and N core-hole lifetimes for the elements Nb–Te (Z=41–52), *Phys. Rev. B*, 1981, **24**, 7121.